Joint Centre for Mesoscale Meteorology, Reading, UK

The Semigeostrophic Diagnosis of Vertical Motion

Part II: Results for an idealised baroclinic wave life cycle

M. A. Pedder
A. J. Thorpe

Internal Report No. 95

September 1998

Met Office Joint Centre for Mesoscale Meteorology Department of Meteorology
University of Reading PO Box 243 Reading RG6 6BB United Kingdom
Tel: +44 (0)118 931 8425 Fax: +44 (0)118 931 8791
www.metoffice.com

Designed and produced by the Met Office © Crown copyright 2001 01/0240 The Met Office logo is a registered trademark.

The Semigeostrophic Diagnosis of Vertical Motion. Part II: Results for an idealised baroclinic wave life cycle

Alan J. Thorpe[1] and Mike A. Pedder

Department of Meteorology, University of Reading

Revised: 21 September 1998

Abstract:

In this paper we apply the method of solution of the semigeostrophic (SG) omega equation developed in Part I to data generated from a numerical simulation of an idealised dry adiabatic frictionless baroclinic wave life cycle. The aim is to compare quantitatively the quasigeostrophic (QG) and SG solutions for the vertical motion and to relate these to the model vertical motion field. This comparison allows an evaluation of how practical, and accurate, it would be to use such balance theories to estimate vertical motion from atmospheric data. It is found that the QG solution tends to overestimate both ascent and descent in the cyclone. This overestimation is due both to an overestimation of the forcing and to a poor treatment of the large horizontal gradients of static stability produced as the tropopause descends near the cyclone centre. As the SG theory more faithfully represents the Ertel-Rossby potential vorticity (PV), the vertical motion which is implied by this distribution of PV is also quantitatively more similar to the model vertical motion than that produced by the QG theory. The PV distribution affects the vertical motion via the forcing and via explicit account of horizontal gradients of the local static stability distribution which appear in the differential operator in the omega equation. The residual between the vertical motion predicted by the SG, or any other balance, theory and that given by the model is produced partly by any inertia-gravity wave activity and partly by inaccuracies in the assumed balance condition.

[1] Corresponding Author: Dept of Meteorology, University of Reading, PO Box 243, Reading RG6 6BB, UK.

1. Introduction

It is well established that synoptic, and other routine, observations of the atmosphere cannot provide accurate estimates of the vertical motion. This is of concern because of the importance of vertical motion in significant and severe weather formation. Numerical weather prediction involves a process of data assimilation which creates an initialised gridded data-set suitable for numerical forecasting. Such forecast data-sets include vertical motion. Understanding synoptic evolution involves establishing essentially simple dynamical theory with which to interpret either the numerical model data or the observations themselves. A test of these theories is to compare their prediction of vertical motion with that produced in numerical models. This is the aim of this paper.

The class of theory to be discussed here is usually referred to as "balanced models". These models claim to explain a significant portion of the vertical motion with the unexplained residual being accounted for by gravity waves. We provide here an in-depth assessment of the balanced model predictions to establish confidence that the next step of isolating the gravity wave component is a valid one. However we do not here evaluate the gravity wave field, leaving that to future research along these lines. Balanced models are conceptually simpler than, say, the primitive equations, but they may be as complicated to solve mathematically. The conceptual simplification is crucial in providing a framework with which to understand the atmosphere. In certain circumstances balanced models, due to the dynamical contstraints imposed in their formulation, may produce predictions that are **more** believable than those from full numerical weather prediction models. At least they allow a check on the dynamical consistency of the full model. In addition, via the building blocks encapsulated in the balanced models, they provide human forecasters with concepts to interpret and communicate forecast model output.

Quasigeostrophic (QG) theory provides a basic framework for the dynamical understanding of extra-tropical development. An example of its use, pertinent to this paper, is given in Rotunno et al 1994 where a numerical simulation of an idealised baroclinic wave is analysed with QG concepts. In particular Q-vectors were calculated from the numerical model pressure field to illuminate both the forcing of vertical motion and for diagnosing frontogenesis. Implicit in the study by Rotunno et al 1994 is the notion that it is not necessary to solve the QG omega equation but rather it is sufficient to compare the forcing of the QG vertical motion with the model vertical motion. The conclusion of that paper is that the QG model provides the essential qualitative understanding of the dynamics of the simulated cyclone life cycle. It is a goal of the work reported here to carry out a quantitative analysis to complement the many qualitative studies carried out previously e.g. Hoskins and Pedder 1980, Rotunno et al 1994. Exceptions to the dearth of quantitative comparisons are Bosart and Lin 1984, Keyser et al 1992 and Pinot et al 1996.

It is important to provide a clear dynamical interpretation of the vertical motion predicted by the QG, or any other balance, theory. The formulation of balance theories is such that a part, or all, of the non-divergent (rotational) flow and temperature is associated with the potential vorticity relevant to that theory via a potential vorticity inversion operation. The dynamical significance of the potential vorticity is that it is the quantity that is conserved according to the assumptions of the theory. Note that each balance theory has a different potential vorticity quantity, each of which has a lesser or greater similarity to the Ertel-Rossby potential vorticity. The associated rotational flow and temperature distributions determine the forcing of the divergent flow and in particular the vertical motion field. In the QG theory this relationship is via an omega equation. It is clear from this that it is the potential vorticity that determines a fraction of the actual rotational and divergent flow. How large this fraction is will depend on how closely the actual motion satisfies the assumed balance condition. One can refer to the part of the motion and temperature field predicted by the

balance theory as being "slaved" to the relevant potential vorticity distribution.

In Part I of this paper the extension to QG theory embodied in semigeostrophic (SG) theory is discussed in detail. The point is made that for a baroclinic wave cyclone the strong horizontal variations in static stability, and potential vorticity, imply that QG theory is strictly outside its range of validity. Furthermore SG theory is the natural counterpart to QG theory in that it retains the simplicity of formulation of the QG theory whilst extending its range of validity significantly to quasi two-dimensional regions of the flow with Rossby number of order unity. In Part I we explored a practical method of evaluating the SG forcing of vertical motion for arbitrary pressure input data. In this paper we apply the method to the baroclinic life-cycle problem. We use the model described by Rotunno et al 1994 and the reader is directed to that paper for the numerical model and formulation details. Here only those aspects of the model and simulation will be discussed which are pertinent to the QG and SG vertical motion calculations. The model integration and the subsequent diagnosis was carried out on a grid of 40 x 80 x 60 points with a resolution of 100 x 100 x 0.25 km.

2. Comparison between SG and QG predictions of vertical motion

In this section we examine the vertical circulations diagnosed using quasigeostrophic and semigeostrophic theories with particular attention to days 6 and 7 of the model integration. At day 7 the Jacobian of the geostrophic momentum (GM) co-ordinate transformation was found to be of order zero or negative in some regions of strong negative shear on the periphery of the simulated cyclone in the lower troposphere. The adjustment scheme described in Part I was used to modify the model's pressure field so that the minimum of this Jacobian was nowhere less than 0.3. The impact of the adjustment on the diagnosed geostrophic forcing of vertical velocity was found to be very small (typically less than a few percent) and highly localised, implying that it did not lead to

any serious ambiguity in the interpretation of vertical velocities associated with the geostrophic forcing. All results discussed later refer to an analysis of the adjusted model data.

In the case of the QG omega equation, solutions were obtained using conventional elliptic equation solving methods (successive over-relaxation) assuming cyclic boundary conditions on vertical velocity in the west-east direction and zero vertical motion at the north, south, top and bottom boundaries. A similar procedure was used to solve the SG omega equation, but in this case applied to data sampled on an enhanced (25 km) resolution grid in GM space (see the Appendix for a summary of the basic equations and Part I for details of the solution method). Since the model vertical velocities were found to be contaminated with some grid-point noise, all model and diagnosed vertical velocity data were smoothed using a simple grid-point filter prior to any graphical or statistical comparisons. This removed all variance associated with the gridscale wave (200 km in the horizontal and 500 m in the vertical) but had little impact on wavelength scales greater than 600 km in the horizontal or 1500 m in the vertical.

2.1 The structure of the Potential Vorticity

Balance theories of atmospheric dynamics are based on the dominant role of the potential vorticity. Under the assumptions of such theories potential vorticity is that quantity which is conserved in dry adiabatic frictionless flow and which also determines the distribution of both the rotational and a significant part of the divergent motion. In this paper we have taken the following strategy in the application of balance theory to data which arises from either observations, NWP model or idealised model analyses. The pressure data are taken from the model data set and then the potential vorticity, relevant to the particular balance theory to be used, is calculated. The rotational flow can then be found by direct PV inversion, although this is not done here. Equally the divergent circulation is predicted by the solution of an omega equation which has a forcing

calculated from the pressure field and, in the case of SG theory, has a coefficient of the elliptic operator that is given by the PV itself.

Given the primary role of the PV in balance theory we now show the structure of the potential vorticity of the life-cycle experiment. These structures possess the key instability characteristics from which the baroclinic wave grows. Figures 1 (a) and (b) show a height section along the direction joining the extrema in vertical velocity (approximately south-west to north-east) displaying the PV distributions after day 7 for the Ertel-Rossby (ER) version and the SG PV. The tropopause has a significant sloping region associated with the zonal jet. Initially the model assumes a very simple potential vorticity structure with one value in the troposphere (0.5 PVU) and a different value in the stratosphere (3.5 PVU). The day 7 comparison shows the similarity between the ER and SG PV - the point is that as far as the omega equation is concerned the QG version "sees" only the horizontal average static stability (no picture shown) whereas the SG version sees the full horizontal and vertical variation of the SG PV. Furthermore we see that the spatial variation in SG PV is very similar to that of the full Ertel-Rossby potential vorticity. Hence this encourages one to expect that the vertical motion predicted by the SG theory will include the effects of these horizontal variations in PV, which are especially evident near the tropopause.

There is however another important feature shown by figure 1 (a). Near the surface, in the zone of large cyclonic vorticity associated with the front, there is an anomaly of Ertel-Rossby potential vorticity. The model has no explicit frictional process so it is producing this anomaly spuriously from the finite difference scheme with its implicit numerical dissipation. This feature is even more evident in the semigeostrophic potential vorticity distribution in Figure 1 (b) where there is a local dipole of SG PV within which SG PV is locally negative. This negative feature is not present in the Ertel PV field although there is a local maximum, i.e. half of the dipole. This region of negative SG PV implies a region of slantwise instability, at least as perceived by the

semigeostrophic theory. As the SG PV appears as a coefficient in the operator of the semigeostrophic omega equation (see Part I) this region of negative values must be removed to make the equation elliptic and for it to have a unique solution. A way to carry out this removal is to simply set the values of SG PV to a default small, but positive, value. This has been the approach used here with a default value of 0.03 PVU. (Note that in this paper when we refer to the sign of the potential vorticity as having dynamical significance we are considering the Northern Hemisphere. The proper criterion, valid in both hemispheres, is that it is the sign of the Coriolis parameter times the potential vorticity that must be positive for ellipticity of the SG omega equation.)

As we will be comparing QG and SG theory it is of interest to compare the relevant potential vorticity distributions. The QG and SG potential vorticities are calculated from the pressure field data provided by the simulation at day 7 using the definitions given in the Appendix. As the QG PV is a quantity that represents a perturbation to a horizontally uniform stratified atmosphere, it is convenient to construct similar quantities for the SG and Ertel-Rossby versions. An appropriate quantity for comparison purposes is a normalised potential vorticity, PV_n, defined by Equation (A7) of the Appendix, which is obtained by dividing the ER PV by its horizontal-average. Note that this quantity is that part of the PV that is associated with the flow and temperature departing from horizontal homogeneity i.e. there is another part of the PV that induces the horizontal mean stratification. This normalised PV quantity "induces" both the balance rotational and divergent flow so it is the ultimate source of the structure of the vertical motion that we are going to study here. (Note, however, that it is not a conserved quantity.) In Figure 1 (d) the normalised SG potential vorticity, P_n, distribution is shown to be very similar to the Ertel-Rossby form, PV_n, in Figure 1 (c), and it also has a similarity to the QG counterpart, q, in Figure 1 (e). However q under-estimates the maximum at the tropopause fold and greatly over-estimates the

amplitude of the negative anomaly associated with the high tropopause over the southern portion of the domain. The point we wish to bring out is that by plotting these quantities in this way one can see how the three estimates of potential vorticity compare with each other. They are indeed comparable qualitatively but exhibit substantial quantitative differences.

A consistent alternative to the methodology pursued here would be to equate the SG PV or the QG PV to the Ertel-Rossby PV, given in Figure 1(a) or (c), rather than as done here to calculate them from the model wind and temperature fields. Then the potential vorticity distributions would have to be inverted to find the pressure and related temperature fields consistent with whichever balance condition was being assumed. This PV inversion approach has not been taken here because we aim to compare with the QG model for which such an association between Ertel-Rossby PV and the QG PV is far from obvious. Furthermore it is not the approach that has been taken by previous authors.

2.2 Statistical inter-comparison for days 6 and 7

Using a normal mode perturbation to the basic state and integrating forward in time the numerical simulation develops a "classical" life cycle of a baroclinic wave. By day 6 the perturbation has grown sufficiently to be noticeable in the surface pressure field. A further day later, at day 7, there is a fully developed intense cyclone wave. Figure 2 shows a horizontal section at the surface of pressure and temperature contours at day 7 including the central box over which the fields will be examined. This shows the stage of development of the wave in its life cycle.

Using the technique described in Part 1 of this paper we now solve the QG and SG omega equations with the model predicted pressure field used as the input. In order to compare the various solutions across the whole domain we follow Pinot et al 1996 and calculate various scatter plots of QG and SG vertical motion against model vertical motion. In addition a statistical analysis will be

presented of the bias and mean error magnitudes.

As noted previously, it has become common practice to infer the QG predicted vertical motion indirectly by looking at the forcing rather than by solving the omega equation to find the vertical motion response itself. It is therefore interesting to compare the correlation between the forcing and the vertical motion solution for the QG system. This is given in Figure 3 in the form of a scatter plot of QG-predicted vertical motion against the QG forcing (i.e. the right-hand-side of equation (A1) in the Appendix) at the same grid point at day 7. For spatially sinusoidal patterns of forcing we would expect there to be a perfect negative correlation between the forcing and the response. From Figure 3 it can be seen that for much of the domain there is a good negative correlation even in the case when the forcing certainly does not have such a simple form. There are, of course, some significant departures to this simple negative correlation.

In Figures 4 (a) and (b) scatter plots of QG and SG solutions are given for day 6. This shows how much closer, in general, the SG solution is to the model vertical velocity compared to the QG prediction. This is true everywhere but especially in regions of descent. Even in the ascent part there is less spread away from the 1-to-1 line for the SG solution. These results are qualitatively similar to those obtained by Pinot et al 1996, in connection with a diagnostic study of a PE simulation of baroclinic development in the ocean. However, our results show much less scatter about the 1-to-1 line than the corresponding comparison in Pinot et al. This we attribute to the more accurate method of SG diagnosis being used in our work (see Part I). In table 1 we show numerical values of the bias; this being defined as the mean of the differences between the QG or SG solution and the collocated model vertical motion in each 1 cm/s bin. In parentheses we also give the mean error magnitudes defined as the average value of the modulus of the error in each bin. Table 1 shows a small bias in the SG solution for ascent greater than 2 cm/s. However the scatter plots and Table 1 shows greater spread for the QG solution than for the SG solution.

By day 7 the cyclone is much more intense with larger vertical motion. In Figure 5 we show various scatter plots. Figures 5 (a) and (b) show that the results at day 7 are similar to those at day 6 in terms of the relative qualitative accuracy of the QG and SG predictions. The scatter plots (Figure 5) suggest the presence of appreciable bias in both the QG and SG solutions for vertical motion in excess of 3 cm/s, though SG is clearly closer to the model solution than QG for all descent points. This is also evident from the error statistics presented in table 2: overall, the SG error is substantially less than the QG error for descent less than 2 cm/s, but comparable in magnitude for ascent greater than 4cm/s. Later figures of the vertical structure of the predicted vertical velocity suggest that a large part of the positive SG bias for ascent greater than 4 cm/s might be attributable to the large positive anomaly in SG vertical motion below a height of 2km. In fact the positive SG solution bias is substantially smaller in the upper troposphere than below 5km, whereas the QG bias tends to be greater at upper levels regardless of the sign of the vertical velocity (see Table 2).

Further insight into the differences between the SG and QG solutions is provided by a similar analysis of the error in the vertical derivative of a predicted vertical velocity field. (Table 3). This supports the idea that most of the positive SG vertical motion bias is associated with anomalously large values of convergence close to the lower boundary, immediately ahead of the surface front and the negative SG PV anomaly (see Figure 1(b)). Elsewhere, the SG divergence bias is substantially smaller than the QG divergence bias, though both solutions tend to over-estimate the magnitude of the model-predicted divergence, regardless of sign. The above comparisons clearly indicate that the SG diagnosis of the ageostrophic circulation is closer to the PE solution than the QG one, especially with respect to the ageostrophic divergence field at upper tropospheric levels, where horizontal gradients of PV and static stability are both large.

In Figure 5 (c) we compare the differences between the QG solution and the model vertical

motion and the same quantity but for the SG solution. It is clear that overall the differences are much smaller for the SG model although, as we have already noted, there are points near the surface front at which the QG solution is closer to the model than is the SG solution.

2.3 Vertical motion structure at day 7

Figure 6 uses the same height section as in Figure 1 to show the QG vertical velocity, the SG vertical velocity and the model vertical velocity. The comparison shows that the QG theory over-emphasises both the ascent and descent, but particularly the ascent, compared with the primitive equation model data. This over-prediction of the QG theory relative to model data has been commented upon by Keyser et al (1992). These authors postulate that the over-prediction is proportional to the square of the Rossby number. In addition they anticipate that higher-order balance models, such as SG theory, might improve upon the QG solution. It is clear from Figure 6 (b) that the SG solution is considerably closer to the model than the QG solution in this cross-section above the near surface layer. Also the maximum QG ascent is at the tropopause whereas it is lower down in the troposphere for the SG and even lower for the model data.

There is however a clear local over-prediction of ascent by the SG model near the surface, even compared with the QG solution. This is the region where SG PV diagnosed from the model data is found to be negative, implying the presence of slantwise instability. This is an example of the local enhancement of vertical motion due to the presence of small stability to slantwise ascent. This behaviour has been previously documented by Thorpe and Emanuel, 1985. The vertical motion enhancement is a real effect if indeed there were to be a local zone of small slantwise stability. However as it does not correspond to such a feature in the model's vertical motion one can either conclude that it is spurious or that the model is not correctly representing slantwise processes. The latter is a very likely possibility as the horizontal resolution of 100km is such that

such mesoscale processes would not be explicitly represented and the model does not have a parametrization of the process. It is therefore a moot point as to which of the SG or the model vertical motion field is "correct" in the near-surface layer. As the primitive equation model is adiabatic and frictionless the potential vorticity should be conserved and so it should remain uniform in the troposphere. This does not happen due to numerical dissipation. Therefore the local positive and negative anomalies created are, in this sense, spurious. They do however have a significant effect on the SG vertical motion pattern. This effect could be removed by imposing uniformity of PV in the SG omega equation. The fact that the QG omega equation does not take into account local PV anomalies means that it locally produces a more believable vertical motion pattern. Therefore the discrepancy between the SG vertical motion and the model pattern does not imply that the SG model is in error in these regions. If the numerical model had been able to conserve PV then the SG model would have produced an accurate estimation.

To more clearly bring out the differences in the two theories we show in Figure 7 the same height section as in Figure 1 but for the difference between the QG and the model vertical motion and the same for the difference between the SG and model vertical motion. These differences represent the component of the vertical motion which is not explained by the particular balance being assumed; this latter being exemplified by the relevant potential vorticity distribution. It will include any inertia-gravity wave contribution within the model-predicted vertical motion field. However using this hydrostatic model of baroclinic instability one might speculate that the gravity wave activity would be very small (see Garner, 1989, for an explanation of this behaviour). More important perhaps is the accuracy of the assumed balance condition. Even in the case of the more accurate SG balance we know that locally highly curved flow will be inaccurately treated and that in such regions a non-linear balance condition should provide a closer approximation to the PE solution. The SG difference field in Figure 7 (b) has a dominant dipole signature on the scale of the

vertical motion itself. This again supports the hypothesis that the differences are not due to a gravity wave signature which, even if it existed, might be expected to be on a smaller horizontal and vertical scale.

To complete the description of the vertical motion predictions in Figure 8 a horizontal section at 5 km of vertical velocity is given for QG, for SG and for the model data. Similar differences between the various solutions can be observed on this section as in the vertical sections.

3. Role of horizontal variations in PV and static stability

It is instructive to analyse the origin of the differences between the QG and SG solutions. In the introduction and in Thorpe (1997) it is seen that the differences must arise from two sources: the different forcing (the right-hand-side of the omega equation) and the role of potential vorticity as a coefficient in the Laplacian operator on the left-hand-side of the equation; see the Appendix and Pedder and Thorpe 1998. We now examine the role of these two effects separately. Furthermore it is possible to take either the QG or the SG omega equation and use the forcing or coefficient suggested by the other theory. In this way we see the impact of the two effects more clearly.

3.1 Sensitivity to the form of the operator

First the sensitivity to the coefficient in the Laplacian operator will be examined without changing the forcing. In Figure 9 (a) contours of vertical motion are shown from the solution of the QG omega equation when the local static stability is taken inside the horizontal derivative operator; here the static stability being used is locally determined and not a horizontal average as in the normal QG system. We call this new vertical velocity the "pseudo-QG omega". There is, in

fact, nothing mathematically incorrect about the pseudo-QG omega equation as it can also be derived by taking the horizontal Laplacian of the QG thermodynamic equation. However it is not possible to derive a potential vorticity conservation equation unless the static stability does not vary in the horizontal. So the solution in Figure 9 (a) is in this sense not consistent with QG PV conservation. It does, on the other hand, include one of the properties that we might imagine lies at the heart of the improved accuracy of the SG system; namely the local dependence on static stability in the operator coefficient. This dependence is provided in the SG omega equation by the use of the SG potential vorticity. Figure 9 (a) suggests that for the QG system the inclusion of a horizontally varying static stability does indeed produce a vertical motion in closer agreement with the model (Figure 6 (c)) than the full QG prediction in Figure 6 (a). Remember though that the inclusion of spatial variations in static stability in the QG theory is formally inconsistent with potential vorticity conservation if one is to consider the time evolution of the QG flow.

We can also investigate this sensitivity to the spatial variation of the coefficient by taking the SG omega equation but replacing the PV with its horizontal average. We call this the "pseudo-SG omega". The solution is shown in Figure 9 (b), which should be compared with the standard SG solution in Figure 6 (b). We would expect that this pseudo-SG vertical motion to be in worse agreement with the model vertical motion than the standard SG solution. For the SG system the role of the horizontally varying PV is very important and leads to significant differences between the solutions in figures 6 (b) and 9 (b). As discussed in Thorpe 1997 the role of the tropopause fold itself can be to create a dipole of forcing with warm air ascending ahead of the fold and descent both in the fold and within the cold air behind the fold. Thorpe 1997 shows that such an effect happens particularly if the frontogenesis is in the form of cold advection combined with confluence. This occurs at the upper front as discussed by Rotunno et al 1994; a process they refer to as the Shapiro effect.

It is instructive to summarise these differences due to the sensitivity to the form of the coefficient by using the scatter plot technique used earlier. In Figure 10 we show the correlations between the vertical motion predicted either by using the locally-varying static stability in the QG operator, Figure 10 (a), or by using the horizontal average PV in the SG model, Figure 9 (b). These figures should be compared with Figure 8 (a) and (b) for the standard QG and SG solutions. As expected, the pseudo-QG vertical motion is in closer agreement with the model vertical motion than the standard QG vertical motion whereas the pseudo-SG is in poorer agreement with the standard SG solution.

3.2 Sensitivity to the form of the forcing

Now the role of the differences in the forcing term for vertical motion is investigated. A simple way to do this is to calculate the QG Laplacian (left-hand-side operator in equation (A1) of the Appendix) of the SG vertical motion solution. This indicates what form the QG forcing would have to take for the QG omega equation to produce the same vertical motion pattern as predicted by the SG system. Figure 11 shows the height section with contours of this "QG form of the SG forcing" for the SG equation. (Note that there is an ambiguity as to how to calculate the vertical numerical- differentiation at the surface. Here we have used a quadratic extrapolation and this leads to the maximum forcing being above the surface. However it is clear that this maximum is at the surface at least for the QG case where we know the forcing explicitly from the divergence of Q. This feature does not however affect the comparison we intend to make here between the various forms of this forcing.) Also shown, for the same section, is the QG forcing. There are significant differences in the forcing of the QG and SG omega equations as indicated by Figure 11. In particular the amplitude of the QG forcing is clearly larger than the pseudo SG forcing and this accounts for the over-prediction by the QG model. Also the QG form of the SG forcing contains

smaller horizontal scale features which are presumably due to the more accurate representation by the SG model of the smaller-scale features associated with the tropopause undulations in the model data. Finally we can evaluate the QG Laplacian of the full model vertical-motion field and this is shown in Figure 11 (c). It is clear by comparing Figure 11 (c) to Figure 11 (b) that the QG and SG models have too large a forcing relative to what would be needed to accurately portray the model vertical motion field. What is perhaps more obvious is that the horizontal scale of the forcing in both the QG and SG models is too large compared to that needed to reproduce the model's vertical velocity.

3.3 Sensitivity to the sign of f.PV

It is clear that near to the surface front the semigeostrophic theory is indicating that there is likely to be at least the potential for symmetric instability as the SG PV is negative there. The SG solution is sensitive to this feature as can be seen by the difference field of vertical motion between the SG and model data, Figure 6 (b). Closer analysis of this feature reveals that there is a large dipole of semigeostrophic forcing with maximum amplitude at the surface in the location where the SG PV is negative (before adjustment). Hence we hypothesize that the reason for the larger difference between SG and model compared to QG and model, in that location, is attributable to the amplitude of the forcing. This feature does not appear to be so significant for the QG model because it is the sign of the horizontally-averaged static stability that determines ellipticity for that model and this does not sense any local zone of static instability even if it were present. The fact that the SG model highlights this region is of significance because it is likely that the resolution of the discretized primitive equation model is not sufficient to resolve symmetric instability so it is incorrectly treating the dynamics in this region. The QG model is much less discriminating in this respect. By day 7 the cyclone in this life-cycle experiment has unrealistic surface features because

the surface winds are very large indicating that surface friction, which has been neglected in the model equations, must play a significant role in real cyclones by this time. We have ascertained that it is the SG forcing term rather than the SG PV as a coefficient in the omega equation that leads to this feature. However this is unlikely to be a generally valid statement as it is well known that extensive regions of negative potential vorticity away from the surface does lead to significant amplification of the vertical motion response (see, for example, Emanuel et al 1987).

4. Concluding Remarks

In this two-part paper we have carried out what we believe to be the first comprehensive quantitative evaluation of the quasi and semigeostrophic prediction of vertical motion for an extra-tropical cyclone. To do this in Part I a full analysis was made of an appropriate and accurate method necessary to produce faithful solutions of the SG omega equation. The point was made that it is not sufficient, as has been done previously, to apply a naïve solution method but that if the method proposed in Part I is used then it becomes straightforward to find the SG solution.

In this part the comparison between the QG and SG vertical motion and the model, or "real", vertical motion has been made. It has been shown that:

- It is mathematically straightforward to evaluate the vertical motion prediction from balance models rather than being satisfied with only the forcing which, in certain circumstances, will give a poor impression of the local vertical motion response.
- The predicted vertical motion should be interpreted as being that part of the vertical motion that can be attributed to the potential vorticity structure and balance condition of a given balance model. Differences with the "real" vertical motion can be due both to the presence of inertia-gravity waves and to inaccuracies in the balance-condition being used.

- The QG model has a potential vorticity distribution, which has significant differences to the anomalies exhibited by the Ertel-Rossby potential vorticity, and an associated vertical motion pattern which substantially over-predicts both the ascent and descent amplitudes. This "error" can be thought of as being due to both an overestimation of the forcing and due to the use of a horizontally homogeneous static stability in regions such as the sloping tropopause where that is a poor assumption. On the other hand it is a very robust computation in the sense that it gives a qualitatively accurate solution even when the QG theory is formally invalid.
- The SG model uses a potential vorticity that closely mimics the full Ertel-Rossby potential vorticity field. The associated vertical motion pattern is quantitatively closer to the model vertical motion than its QG counterpart, particularly in regions of descent.
- Both in this paper and in Thorpe 1997 the point is made that the SG model correctly accounts for the role of the strongly sloping tropopause that is typically found in extra-tropical cyclones and elsewhere. The effect of the strong gradients in potential vorticity is to modulate on the mesoscale the synoptic scale patterns of vertical motion that otherwise are well represented by QG theory.
- Unlike the QG omega equation, the SG omega equation shows that different dynamics must apply in regions where the potential vorticity has the opposite sign to the Coriolis parameter. Whilst physically this is to be expected (due to the presence of symmetric instability in such circumstances) it means that care has to be exercised to adjust the pressure data to extend the solution into such regions. This is an important feature of the semigeostrophic model providing considerably more dynamical insight than its quasigeostrophic counterpart.

It remains for future work to investigate if the use of a higher order balance than that in SG theory would allow an evaluation of the inertia-gravity wave component of the flow to be made. A

candidate is the so-called semi-balance system described by Raymond 1992 based on non-linear balance. A disadvantage of the semi-balance system is that there appears to be no simple analogue to the omega equation that does not involve evaluating time derivatives. Also it is important to test the accuracy of the SG model using observed pressure data for real extra-tropical cyclones.

Acknowledgements

The authors would like to thank Dr Rich Rotunno for providing the numerical model, Dr Ed Dicks for substantial programming support during this research and Michal Ziemianski for helpful comments on the manuscript.

Appendix

Here the main equations used in this studied are summarised. Full description of the notation and derivation is given in Part I. The quasigeostrophic omega equation is:

$$\overline{N^2}\nabla_h^2 w + f^2\frac{\partial^2 w}{\partial z^2} = F = 2\nabla_h \cdot \mathbf{Q} \qquad \text{(A1)}$$

where

$$\mathbf{Q} = \left(-\frac{g}{\theta_o}\left(\frac{\partial u_g}{\partial x}\frac{\partial \theta}{\partial x} + \frac{\partial v_g}{\partial x}\frac{\partial \theta}{\partial y}\right), -\frac{g}{\theta_o}\left(\frac{\partial u_g}{\partial y}\frac{\partial \theta}{\partial x} + \frac{\partial v_g}{\partial y}\frac{\partial \theta}{\partial y}\right)\right) \qquad \text{(A2)}$$

The quasigeostrophic potential vorticity is defined by:

$$q = \zeta_g + \frac{\partial}{\partial z}\left(\frac{f}{\overline{N^2}}\frac{g}{\theta_0}\left(\theta - \bar{\theta}\right)\right) \qquad \text{(A3)}$$

where overbar here and elsewhere refers to a horizontal average. The semigeostrophic omega equation is

$$\frac{g}{f\theta_o}\nabla_H^2 P w^* + f^2\frac{\partial^2 w^*}{\partial Z^2} = F^* = 2\nabla_H \cdot \mathbf{Q}^* \qquad \text{(A4)}$$

where $X = x + \frac{v_g}{f}$ $\quad Y = y - \frac{u_g}{f}$ $\quad Z = z$, $\underline{\nabla}_H = \left(\frac{\partial}{\partial X}, \frac{\partial}{\partial Y}\right)$, $w^* = (w/J)$ and $P = \zeta_g^* \frac{\partial \theta}{\partial Z}$ is the SG potential vorticity. In (A4), the SG **Q**-vector is defined by

$$\mathbf{Q}^* = \left(-\frac{g}{\theta_o}\left(\frac{\partial u_g}{\partial X}\frac{\partial \theta}{\partial X} + \frac{\partial v_g}{\partial X}\frac{\partial \theta}{\partial Y}\right), -\frac{g}{\theta_o}\left(\frac{\partial u_g}{\partial Y}\frac{\partial \theta}{\partial X} + \frac{\partial v_g}{\partial Y}\frac{\partial \theta}{\partial Y}\right)\right) \qquad \text{(A5)}$$

The Ertel-Rossby potential vortcity is defined by:

$$PV = \underline{\zeta}.\nabla\theta \qquad \text{(A6)}$$

where density has been taken as unity for the Boussinesq approximation. Use is made of a

normalised Ertel-Rossby potential vorticity defined by:

$$PV_n = f\frac{PV}{\overline{PV}} \qquad \text{(A7)}$$

and also of a normalised SG potential vorticity:

$$P_n = f\frac{P}{\overline{P}} \qquad \text{(A8)}$$

References

Bosart, L. F. and Lin, S. C., 1984: A diagnostic study of the President's day storm of February 1979, *Mon. Wea. Rev.*, **112**, 2148-2177.

Emanuel, K. A., Fantini, M. and Thorpe, A. J., 1987: Baroclinic instability in an environment of small stability to slantwise convection. Part 1: Two-dimensional models. *J. Atmos. Sci.*, **44**, 1559-1573.

Garner, S. T., 1989: Fully Lagrangian numerical solutions of unbalanced frontogenesis and frontal collapse. *J. Atmos. Sci.*, **46**, 717-739.

Hoskins, B. J. and Pedder M. A., 1980: The diagnosis of middle latitude synoptic development. *Q. J. R. Meteorol. Soc.*, **106**, 707-719.

Keyser, D., Schmidt, B. D. and Duffy, D. G., 1992: Quasigeostrophic diagnosis of three-dimensional ageostrophic circulations in an idealised baroclinic disturbance. *Mon. Wea. Rev.*, **120**, 698-730.

Pedder, M. A. and Thorpe, A. J., 1998: The semigeostrophic diagnosis of vertical motion. Part I: Formulation and Co-ordinate transformations. *Q. J. R. Meteorol. Soc.*, **124**, submitted.

Pinot, J-M., Tintore, J. and Wang, D-P., 1996: A study of the omega equation for diagnosing vertical motions at ocean fronts. *J. Marine Res.*, **54**, 239-259.

Raymond, D. J., 1992: Nonlinear balance and potential-vorticity thinking at large Rossby number, *Q. J. R. Meteorol. Soc.*, **118**, 987-1015.

Rotunno, R., Skamarock, W. C. and Snyder, C., 1994: An analysis of frontogenesis in numerical simulations of baroclinic waves. *J. Atmos. Sci.*, **51**, 3373-3398.

Thorpe, A. J. and Emanuel, K. A., 1985: Frontogenesis in the presence of small stability to slantwise convection. *J. Atmos. Sci.*, **42**, 1809-1824.

Thorpe, A. J., 1997: Attribution and its application to mesoscale structure associated with tropopause folds. *Q. J. R. Meteorol. Soc.*, **123**, 2377-2399.

TABLES

	Lower		Upper		All	
PE	SG	QG	SG	QG	SG	QG
-3 to –2	+0.13 (*0.17*)	+0.04 (*0.22*)	-0.04 (*0.13*)	-0.36 (*0.38*)	+0.08 (*0.16*)	-0.08 (*0.28*)
-2 to –1	+0.16 (*0.21*)	+0.11 (*0.27*)	+0.04 (*0.17*)	-0.16 (*0.27*)	+0.11 (*0.19*)	+0.00 (*0.27*)
-1 to 0	+0.03 (*0.07*)	+0.02 (*0.09*)	+0.02 (*0.06*)	+0.01 (*0.06*)	+0.03 (*0.06*)	+0.01 (*0.07*)
0 to +1	-0.05 (*0.07*)	-0.03 (*0.09*)	-0.02 (*0.05*)	-0.00 (*0.06*)	-0.03 (*0.06*)	-0.01 (*0.07*)
+1 to +2	-0.06 (*0.21*)	-0.05 (*0.31*)	+0.01 (*0.22*)	+0.14 (*0.37*)	-0.03 (*0.22*)	+0.03 (*0.33*)
+2 to +3	+0.12 (*0.24*)	+0.00 (*0.29*)	+0.17 (*0.27*)	+0.22 (*0.38*)	+0.14 (*0.24*)	+0.07 (*0.31*)

Table 1: Mean error, or bias, and mean error magnitude (in parenthesis) of the vertical velocity (cm/s) diagnosed from QG and SG solutions at day 6, within the intervals of PE vertical velocity shown in column 1. In the column headings, 'Lower' refers to the layer 0.5 to 5.0 km, 'Upper' refers to the layer 5 to 10.0 km and 'All' refers to the layer 0.5 to 10.0 km. (Statistics calculated from data sampled over horizontal 4000 km × 4000 km domain.)

	Lower		Upper		All	
PE	SG	QG	SG	QG	SG	QG
-8 to –6	-0.47 (*0.52*)	-3.30 (*3.30*)	-0.49 (*0.53*)	-3.73 (*3.73*)	-0.47 (*0.52*)	-3.41 (*3.41*)
-6 to –4	-0.15 (*0.58*)	-1.51 (*1.63*)	-0.02 (*0.32*)	-2.09 (*2.09*)	-0.10 (*0.49*)	-1.73 (*1.80*)
-4 to –2	+0.12 (*0.59*)	-0.32 (*0.93*)	+0.13 (*0.39*)	-0.61 (*0.77*)	+0.13 (*0.51*)	-0.44 (*0.87*)
-2 to 0	+0.04 (*0.20*)	+0.07 (*0.23*)	+0.03 (*0.16*)	+0.02 (*0.15*)	+0.03 (*0.18*)	+0.04 (*0.18*)
0 to +2	-0.16 (*0.26*)	-0.05 (*0.24*)	-0.05 (*0.14*)	+0.00 (*0.12*)	-0.09 (*0.19*)	-0.02 (*0.17*)
+2 to +4	+0.28 (*1.17*)	+0.38 (*1.28*)	+0.07 (*0.65*)	+0.46 (*0.96*)	+0.19 (*0.94*)	+0.42 (*1.14*)
+4 to +6	+1.50 (*1.82*)	+1.44 (*1.86*)	+0.74 (*0.93*)	+1.59 (*1.75*)	+1.20 (*1.45*)	+1.50 (*1.82*)
+6 to +8	+2.78 (*2.78*)	+2.64 (*2.64*)	+1.75 (*1.75*)	+2.76 (*2.76*)	+2.47 (*2.47*)	+2.67 (*2.67*)

Table 2: Mean error, or bias, and mean error magnitude (in parenthesis) on vertical velocity (cm/s) diagnosed from QG and SG solutions at day 7, within the intervals of PE vertical velocity shown in column 1. Other details as in table 1.

	Lower		Upper		All	
PE	SG	QG	SG	QG	SG	QG
-3 to –2	-0.34 (*0.51*)	-1.23 (*1.26*)	-0.28 (*0.31*)	-0.92 (*0.92*)	-0.33 (*0.46*)	-1.15 (*1.18*)
-2 to –1	-0.11 (*0.32*)	-0.35 (*0.56*)	-0.43 (*0.51*)	-0.56 (*0.65*)	-0.26 (*0.41*)	-0.46 (*0.60*)
-1 to 0	-0.01 (*0.08*)	+0.00 (*0.08*)	+0.03 (*0.09*)	-0.00 (*0.09*)	+0.01 (*0.09*)	-0.00 (*0.08*)
0 to +1	-0.01 (*0.13*)	-0.01 (*0.13*)	-0.01 (*0.10*)	-0.01 (*0.11*)	-0.01 (*0.12*)	-0.01 (*0.12*)
+1 to +2	+0.34 (*0.71*)	+0.43 (*0.70*)	+0.15 (*0.31*)	+0.81 (*0.82*)	+0.25 (*0.52*)	+0.61 (*0.76*)
+2 to +3	+0.91 (*1.19*)	+0.75 (*0.89*)			+0.91 (*1.19*)	+0.75 (*0.89*)
+3 to +4	+2.17 (*2.18*)	+1.55 (*1.55*)			+2.17 (*2.18*)	+1.55 (*1.55*)

Table 3: Mean error, or bias, and mean error magnitude (in parenthesis) on $\partial w/\partial z$ (units 10^{-5} s^{-1}) diagnosed from QG and SG solutions at day 6, within the intervals of PE values shown in column 1. Blank cells indicate sample size too small for reliable estimation. Other details as in Table 1.

Figure Captions

Figure 1: **(a)** A height section along the direction joining the extrema in vertical velocity showing the PV distribution (viewed looking toward the north-west, i.e., with the south-west on the left-hand-side) after day 7 for the Ertel version (contour interval: 1PVU for PV≥1PVU and 0.2 PVU for PV<1 PVU with values less than 1 PVU given by dashed contours), **(b)** height section of the SG PV (same contour interval as in (a)), **(c)** height section of normalised potential vorticity PV_n, defined by Equation (A7) (contour interval: 0.5 f with the bold contour being f and dashed contours representing values less than f), **(d)** same section, and contour interval, for the SG normalised quantity P_n, defined by Equation (A8) and **(e)** same section, and contour interval, for the QG quantity q, given by Equation (A3).

Figure 2: Horizontal section at the surface showing contours of pressure (contour interval 3 mb) and temperature (contour interval 3 K) at day 7 including the central box over which the fields will be examined. This shows the evolution of the wave at this stage in its life cycle.

Figure 3: Scatter plot of the QG forcing function versus the QG vertical motion response at day 7.

Figure 4: **(a)** Scatter plot of QG vertical motion against model vertical motion for day 6 and **(b)** the same for SG versus the model.

Figure 5: **(a)** Scatter plot of QG vertical motion against model vertical motion at day 7, **(b)** the same for SG versus the model, and **(c)** the same for the difference between the QG solution and the model vertical motion versus the difference between the SG solution and the model vertical motion.

Figure 6: **(a)** The same height section as in Figure 1 showing the QG vertical velocity, **(b)** the SG vertical velocity and **(c)** the model vertical velocity (contour interval = 2 cm/s, with negative values dashed).

Figure 7: **(a)** The same height section as in Figure 1 showing the difference between the QG and the model vertical motion and **(b)** the same for the difference between the SG and model vertical

motion (contour interval = 1 cm/s).

Figure 8: **(a)** Horizontal section at 5km of vertical velocity for QG, **(b)** for SG and **(c)** for the model data.

Figure 9: **(a)** Same height section as in Figure 1 showing contours of vertical motion for QG when the static stability is taken inside the horizontal derivative operator and **(b)** Same for SG but where the PV is replaced by its horizontal average.

Figure 10: **(a)** Scatter plot of the vertical motion for QG, when the static stability is taken inside the horizontal derivative operator, against the model vertical motion and **(b)** of the vertical motion for SG but where the PV is replaced by its horizontal average.

Figure 11: **(a)** The same height section as in Figure 1 showing contours of the "QG form of the SG forcing" relevant for the QG equation. The QG form of the SG forcing is found by evaluating the QG Laplacian of the SG vertical motion solution, **(b)** same section for the QG forcing itself and **(c)** the forcing produced if the QG Laplacian of the full model vertical motion field is evaluated (contour interval $1\text{x}10^{-16}\,\text{m}^{-1}\,\text{s}^{-3}$, negative contours are dashed).

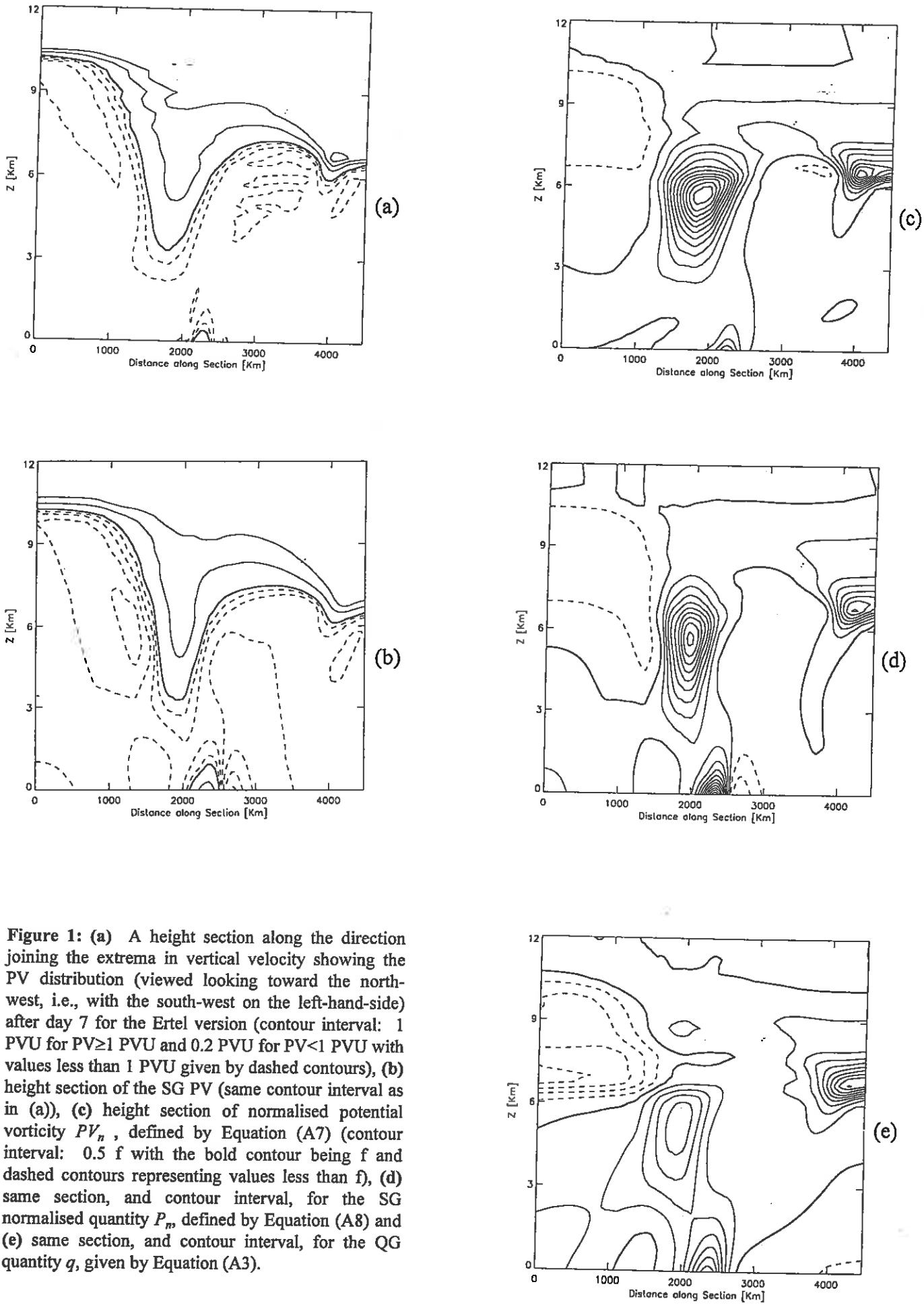

Figure 1: (a) A height section along the direction joining the extrema in vertical velocity showing the PV distribution (viewed looking toward the north-west, i.e., with the south-west on the left-hand-side) after day 7 for the Ertel version (contour interval: 1 PVU for PV≥1 PVU and 0.2 PVU for PV<1 PVU with values less than 1 PVU given by dashed contours), **(b)** height section of the SG PV (same contour interval as in (a)), **(c)** height section of normalised potential vorticity PV_n , defined by Equation (A7) (contour interval: 0.5 f with the bold contour being f and dashed contours representing values less than f), **(d)** same section, and contour interval, for the SG normalised quantity P_n, defined by Equation (A8) and **(e)** same section, and contour interval, for the QG quantity q, given by Equation (A3).

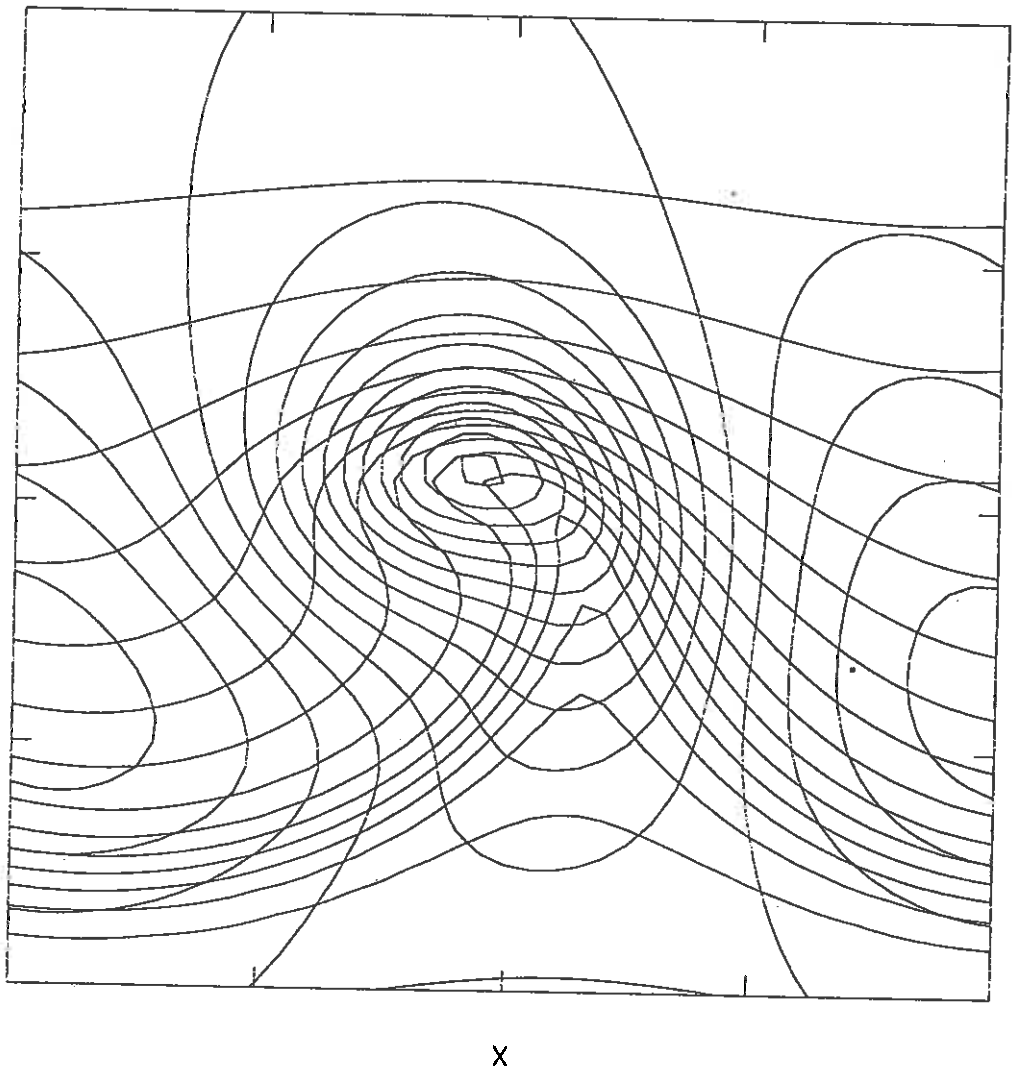

Figure 2: Horizontal section at the surface showing contours of pressure (contour interval 3 mb) and temperature (contour interval 3 K) at day 7 including the central box over which the fields will be examined. This shows the evolution of the wave at this stage in its life cycle.

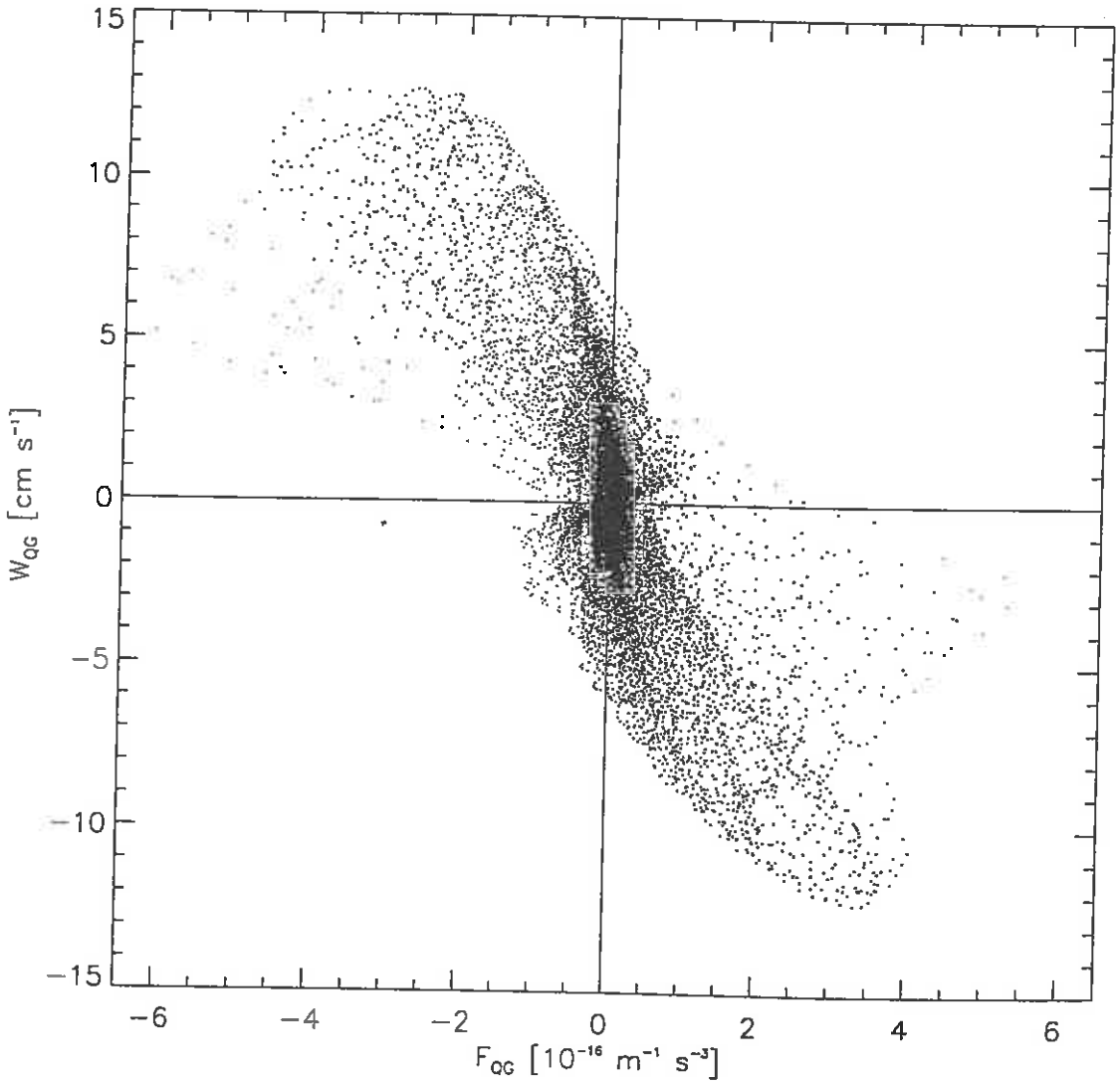

Figure 3: Scatter plot of the QG forcing function versus the QG vertical motion response at day 7.

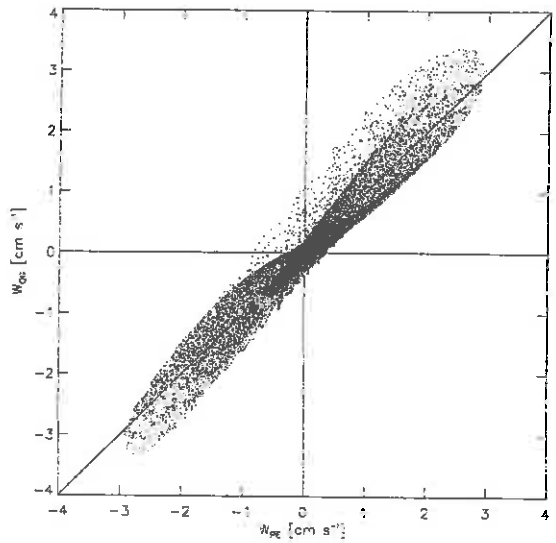

(a)

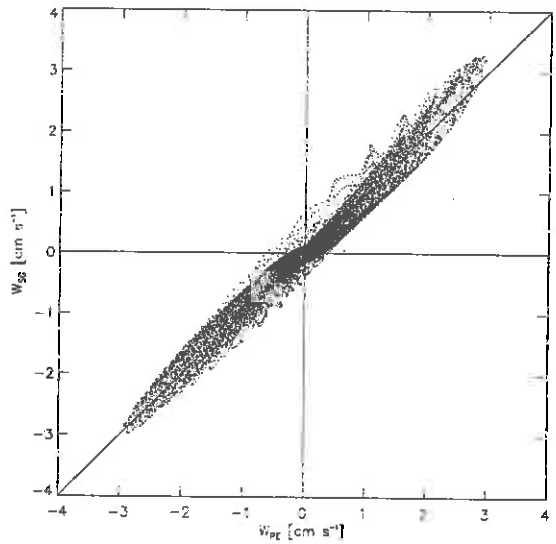

(b)

Figure 4: (a) Scatter plot of QG vertical motion against model vertical motion for day 6 and **(b)** the same for SG versus the model.

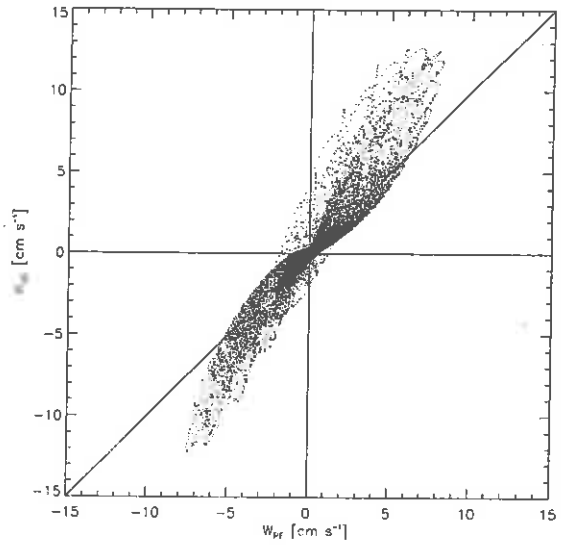

(a)

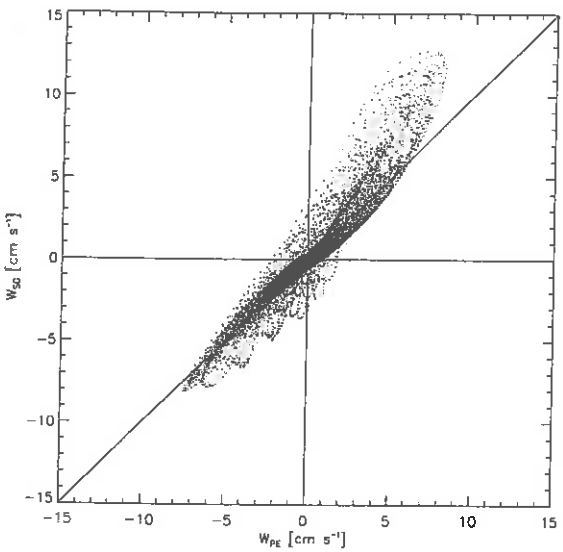

(b)

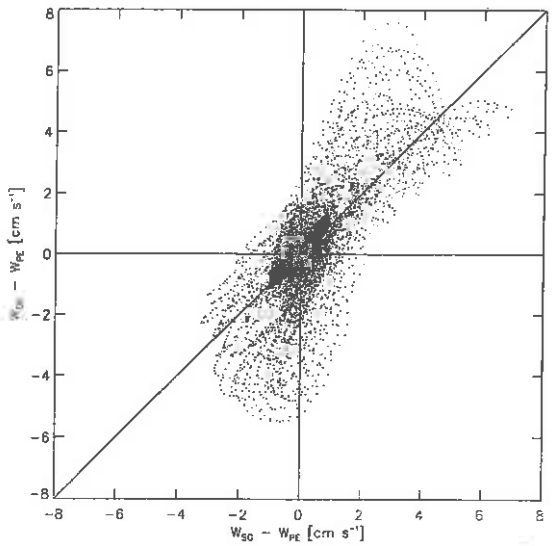

(c)

Figure 5: (a) Scatter plot of QG vertical motion against model vertical motion at day 7, **(b)** the same for SG versus the model, and **(c)** the same for the difference between the QG solution and the model vertical motion versus the difference between the SG solution and the model vertical motion.

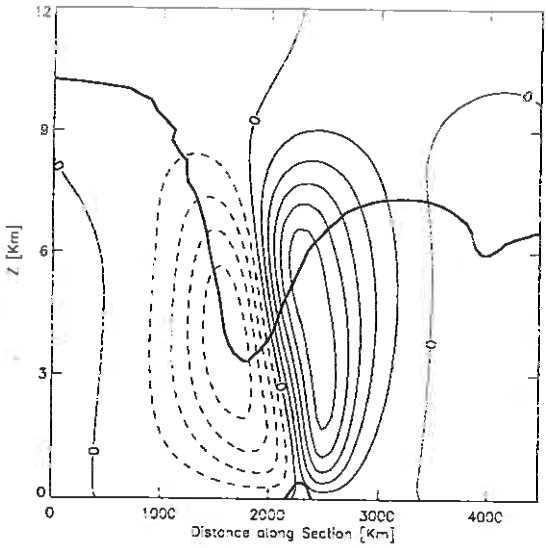

(a)

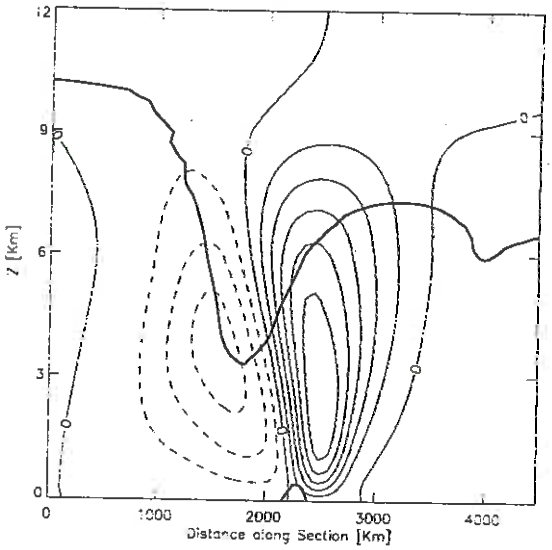

(b)

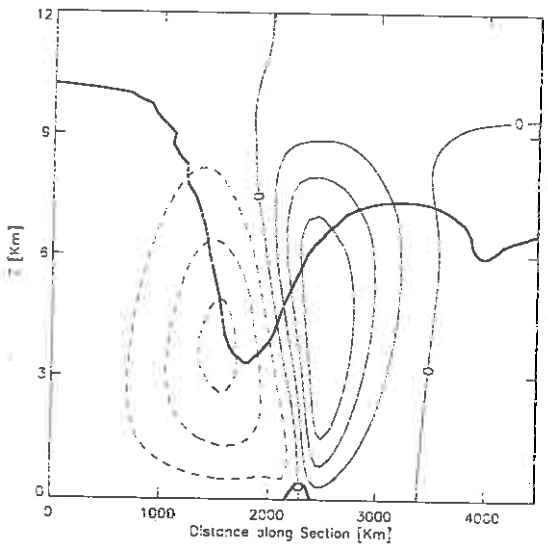

(c)

Figure 6: **(a)** The same height section as in Figure 1 showing the QG vertical velocity, **(b)** the SG vertical velocity and **(c)** the model vertical velocity (contour interval = 2 cm/s, with negative values dashed).

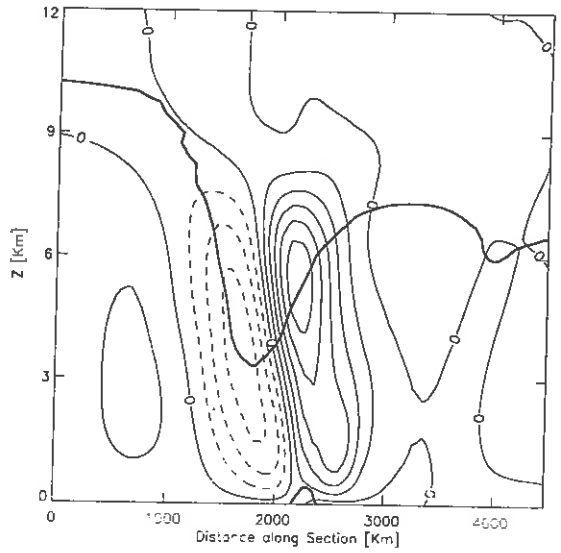

(a)

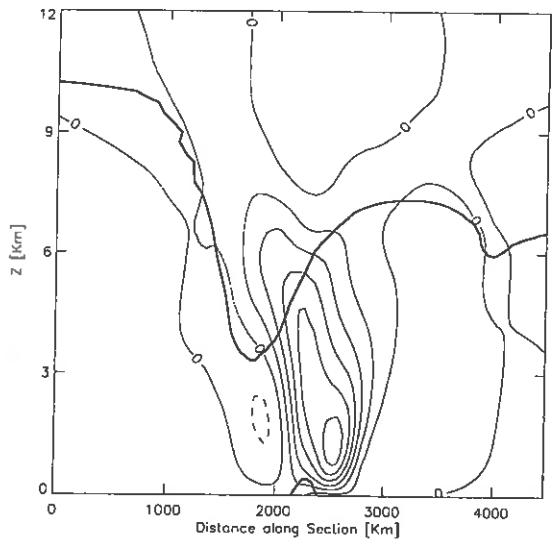

(b)

Figure 7: (a) The same height section as in Figure 1 showing the difference between the QG and the model vertical motion and **(b)** the same for the difference between the SG and model vertical motion (contour interval = 1 cm/s).

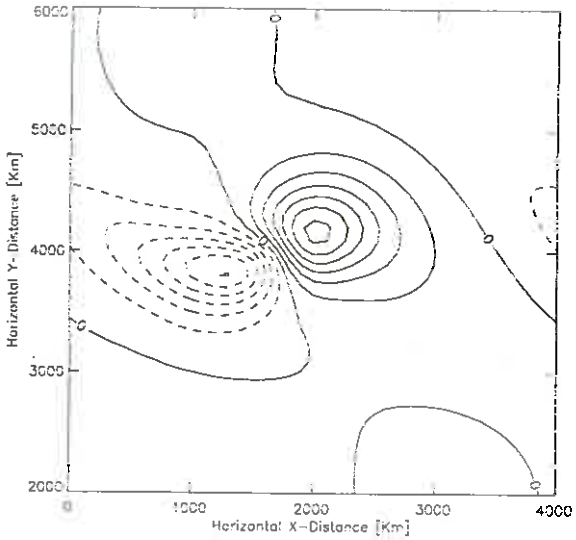

(a)

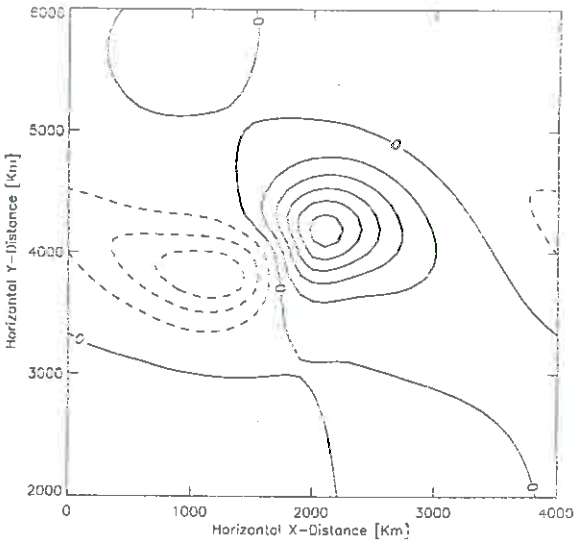

(b)

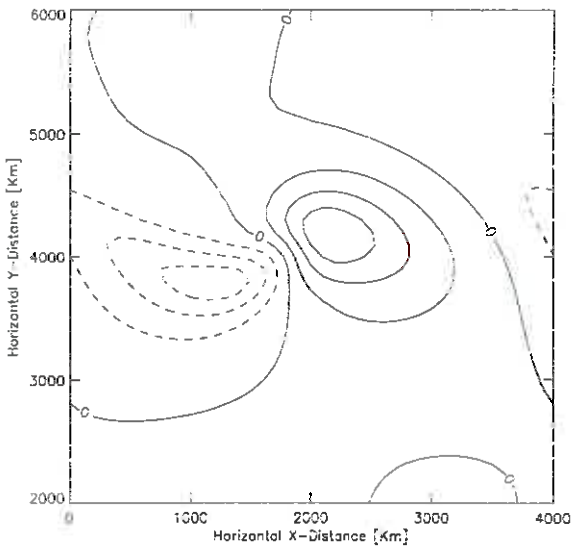

(c)

Figure 8: **(a)** Horizontal section at 5km of vertical velocity for QG, **(b)** for SG and **(c)** for the model data.

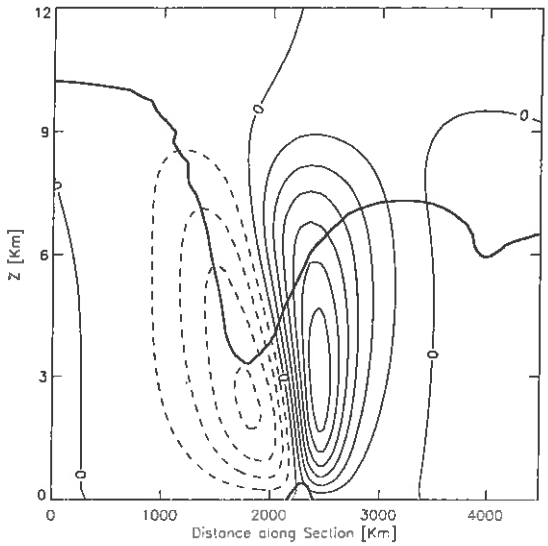

(a)

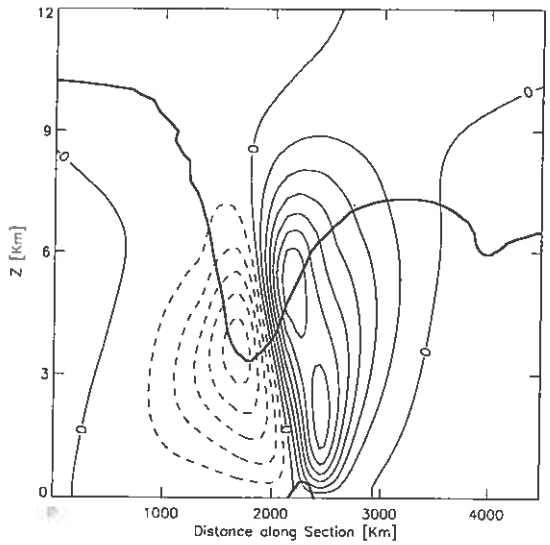

(b)

Figure 9: (a) Same height section as in Figure 1 showing contours of vertical motion for QG when the static stability is taken inside the horizontal derivative operator and **(b)** Same for SG but where the PV is replaced by its horizontal average.

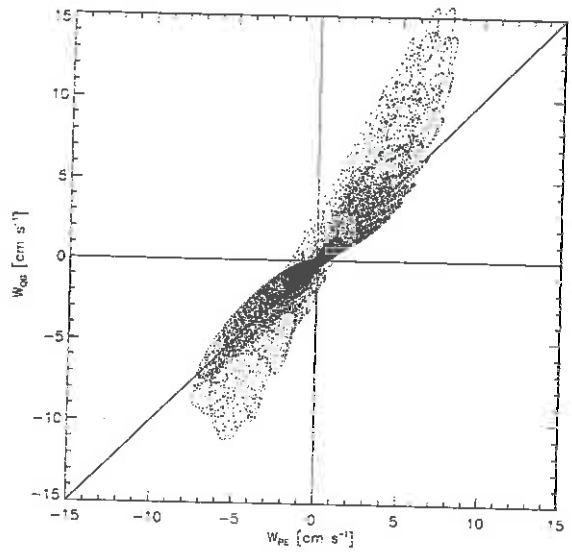

(a)

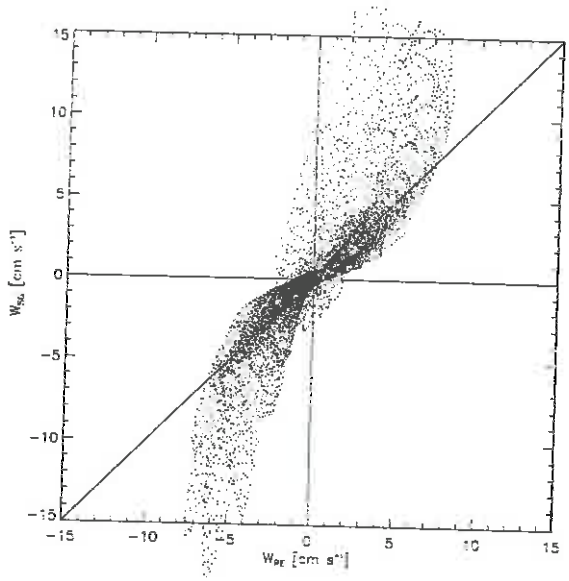

(b)

Figure 10: (a) Scatter plot of the vertical motion for QG, when the static stability is taken inside the horizontal derivative operator, against the model vertical motion and **(b)** of the vertical motion for SG but where the PV is replaced by its horizontal average.

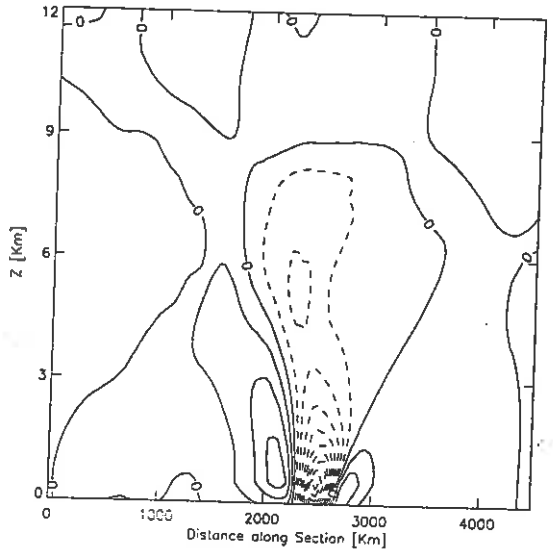

(a)

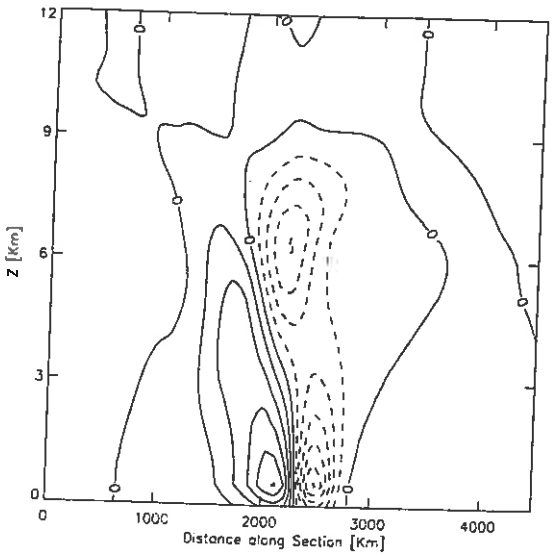

(b)

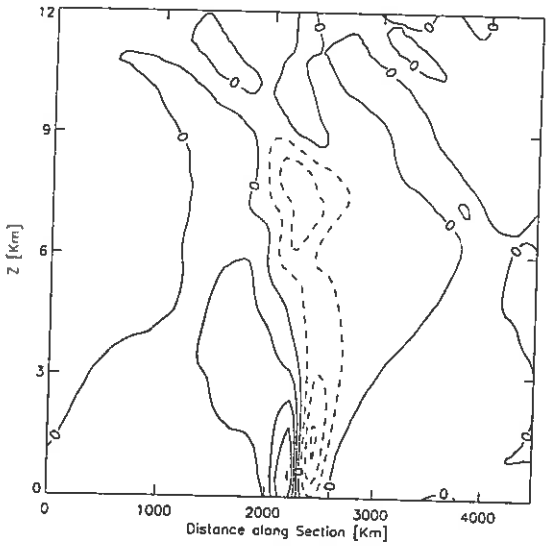

(c)

Figure 11: **(a)** The same height section as in Figure 1 showing contours of the "QG form of the SG forcing" relevant for the QG equation. The QG form of the SG forcing is found by evaluating the QG Laplacian of the SG vertical motion solution, **(b)** same section for the QG forcing itself and **(c)** the forcing produced if the QG Laplacian of the full model vertical motion field is evaluated (contour interval $1 \times 10^{-16}\ m^{-1} s^{-3}$, negative contours are dashed).

CURRENT JCMM INTERNAL REPORTS

This series of JCMM Internal Reports, initiated in 1993, contains unpublished reports and also versions of articles submitted for publication. The complete set of Internal Reports is available from the National Meteorological Library on loan, if required.

1. **Research strategy and programme**
   K A Browning et al
   January 1993

2. **The GEWEX Cloud System Study (GCSS)**
   GEWEX Cloud System Science Team
   January 1993

3. **Evolution of a mesoscale upper tropospheric vorticity maximum and comma cloud from a cloud-free two dimensional potential vorticity anomaly**
   K A Browning
   January 1993

4. **The global energy and water cycle**
   K A Browning
   July 1993

5. **Structure of a midlatitude cyclone before occlusion**
   K A Browning and N Roberts
   July 1993

6. **Developments in systems and tools for weather forecasting**
   K A Browning and G Szejwach
   July 1993

7. **Diagnostic study of a narrow cold frontal rainband and severe winds associated with a stratospheric intrusion**
   K A Browning and R Reynolds
   August 1993

8. **Survey of perceived priority issues in the parametrizations of cloud-related processes in GCMs**
   K A Browning
   September 1993

9. **The effect of rain on longwave radiation**
   I Dharssi
   September 1993

10. **Cloud microphysical processes - a description of the parametrization used in the large eddy model**
    H Swann
    October 1993

11. **An appreciation of the meteorological research of Ernst Kleinschmidt**
    A J Thorpe
    May 1992

12. **Potential vorticity of flow along the Alps**
    A J Thorpe, H Volkert and Dietrich Heimann
    August 1992

13. **The representation of fronts**
    A J Thorpe
    January 1993

14. **A parametrization scheme for symmetric instability: test for an idealised flow**
C S Chan and A J Thorpe
February 1993

15. **The Fronts 92 Experiment: a Quicklook Atlas**
Edited by T D Hewson
November 1993

16. **Frontal wave stability during moist deformation frontogenesis**
Part 1: Linear wave dynamics
C H Bishop and A J Thorpe
May 1993

17. **Frontal wave stability during moist deformation frontogenesis**
Part 2. The suppression of non-linear wave development
C H Bishop and A J Thorpe
May 1993

18. **Gravity waves in sheared ducts**
S Monserrat and A J Thorpe
October 1993

19. **Potential vorticity and the electrostatics analogy: quasi-geostrophic theory**
C Bishop and A J Thorpe
November 1993

20. **Recent advances in the measurement of precipitation by radar**
A J Illingworth
April 1993

21. **Micro-physique et givrage: cloud microphysics and aircraft icing**
A J Illingworth
May 1993

22. **Differential phase measurements of precipitation**
M Blackman and A J Illingworth
May 1993

23. **Estimation of effective radius of cloud particles from the radar reflectivity**
N I Fox and A J Illingworth
May 1993

24. **A simple method of Dopplerising a pulsed magnetron radar**
A Hua, A J Illingworth and J Eastment
November 1993

25. **Radiation and polar lows**
George C Craig
February 1994

26. **Collected preprints submitted to the International Symposium on the Life Cycles of Extratropical Cyclones; Bergen, Norway, 27 June - 1 July 1994**
April 1994

27. **Convective frontogenesis**
Douglas J Parker and Alan J Thorpe
April 1994

28. **Improved measurement of the ice water content in cirrus using a total water evaporator**
Philip R A Brown and Peter N Francis
April 1994

29. **Mesoscale effects of a dry intrusion within a vigorous cyclone**
K A Browning and B W Golding
April 1994

30. **GEWEX Cloud System Study, Science Plan**
May 1994

31. **Parametrization of momentum transport by convectively generated gravity waves**
R Kershaw
May 1994

32. **Mesoscale Modelling Newsletter No 5**
May 1994

33. **Observations of the mesoscale sub-structure in the cold air of a developing frontal cyclone**
K A Browning, S A Clough, C S A Davitt, N M Roberts and T D Hewson
May 1994

34. **Longwave radiative forcing of a simulated tropical squall line**
Imtiaz Dharssi
July 1994

35. **On the nature of the convective circulation at a kata-cold front**
K A Browning
September 1994

36. **Collective preprints of papers submitted to the COST-75 International Seminar on Advanced Weather Radar Systems, Brussels, 20-23 September 1994**
November 1994

37. **Use of satellite imagery to diagnose events leading to frontal thunderstorms: Parts I and II of a case study**
K A Browning and N M Roberts
November 1994

38. **The role of spaceborne millimetre-wave radar in the global monitoring of ice cloud**
P R A Brown, A J Illingworth, A J Heymsfield, G M McFarquhar, K A Browning and M Gosset
December 1994

39. **Potential vorticity inversion**
Michal Ziemianski
October 1994

40. **Theory of mature tropical cyclones; a comparison between Kleinschmidt (1951) and Emanuel (1986)**
Suzanne L Gray
December 1994

41. **Dispersion and removal of pollutants during the passage of an atmospheric frontal system**
N R Gimson
December 1994

42. **The role of snow sublimation in frontogenesis**
D J Parker and A J Thorpe
December 1994

43. **Potential vorticity and the electrostatics Analogy: Ertel-Rossby formulation**
A J Thorpe and C H Bishop
December 1994

44. **Mesoscale aspect of extratropical cyclones: an observational perspective**
K A Browning
January 1995

45. **A polar low outbreak: evolution and mesoscale structures**
T D Hewson, G C Craig and C Claud
February 1995

46. **Generation of near-surface gusts of deep convection**
K Nakamura and R Kershaw
April 1995

47. **Attribution concepts applied to the Omega Equation**
S A Clough, C S A Davitt and A J Thorpe
June 1995

48. **Parametrization of mixed-phase cloud and precipitation**
Susan P Ballard and M Gerard Hutchinson
June 1995

49. **Short-range forecasting of stratocumulus: initialization prediction**
Susan P Ballard, Simon D Jackson and B Macpherson
June 1995

50. **Contributions of the JCMM/Dept of Meteorology Radar Group to the 27th AMS Radar Meteorology Conference, Vail October 1995**
June 1995

51. **Cold pools in shear**
Douglas J Parker
September 1995

52. **High-resolution analysis of frontal fracture**
K A Browning, S P Ballard and C S A Davitt
September 1995

53. **The albedo of broken cloud fields: calculations using a modified two stream radiation code**
Imtiaz Dharssi and Roy Kershaw
October 1995

54. **Parametrization of momentum transport by convection. I: theory and cloud modelling results**
R Kershaw and D Gregory
November 1995

55. **Variation of frontal structure along a cold front**
K A Browning and N M Roberts
November 1995

56. **Secondary frontal waves**
Douglas Parker
December 1995

57. **Objective fronts**
T D Hewson
March 1996

58. **Mesoscale analysis of the activation of a cold front during cyclogenesis**
K A Browning, N M Roberts and A J Illingworth
June 1996

59. **Investigation of different representations of rain in a 1-d evaporation model**
H Swann
May 1996

60. **Parametrization of diabatic processes in the inversion of the omega-equation**
M Athanassiadou and A J Thorpe
June 1996

61. **The role of the environmental flow in the development of secondary frontal cyclones**
I A Renfrew, A J Thorpe and A Joly
June 1996

62. **Consequences of the geostrophic momentum approximation on barotropic instability**
S Malardel, A J Thorpe and A Joly
June 1996

63. **Contributions to the AMS/RMS Conference on Mesoscale Processes**
Reading, 9-13 September 1996

64. **Vorticity and potential vorticity in stratified flows interacting with an isolated obstacle**
Jorge A Gutiérrez and A J Thorpe
September 1996

65. **Triple point development: two case studies**
Douglas Parker
September 1996

66. **Radar observations of wind-shear splitting within evolving atmospheric Kelvin-Helmholtz billows**
D Chapman and K A Browning
April 1997

67. **Cold frontal structure derived from radar wind profilers**
K A Browning, D Jerrett, J Nash, T Oakley and N M Roberts
May 1997

68. **The dry intrusion and its effect on the frontal, cloud and precipitation structure of extratropical cyclones**
K A Browning - Text of invited special lecture at the Spring Conference
of the Meteorological Society of Japan, University of Tsukuba, 22 May 1997

69. **Met. Office Unified Model data, diagnostics, graphics programs, and other observational data available from the JCMM through the aegis of the Universities Weather Research Network (UWERN).** (Plus supplement)
Peter Panagi and Ed Dicks
June 1997

70. **Contributions of the JCMM/Dept of Meteorology Radar Group to the 28th AMS Radar Meteorology Conference.** Austin, Texas
September 1997

71. **Sensitivity of short-range weather forecasts to local potential vorticity modifications**
Meral Demirtas and Alan Thorpe
July 1997

72. **Objective identification of frontal wave cyclones**
T D Hewson
August 1997

73. **Attribution and its application to mesoscale structure associated with tropopause folds**
A J Thorpe
September 1997

74. **The role of the environmental flow in the development of secondary frontal cyclones**
Ian A Renfrew, Alan J Thorpe and Craig H Bishop
September 1997

75. **Potential vorticity: a short history of its definitions and uses**
Alan J Thorpe and Hans Volkert
September 1997

76. **Superposing semi-geostrophic potential vorticity anomalies**
H R Birkett and A J Thorpe
September 1997

77. **Short period forecasting of catchment-scale precipitation.**
Part 1: the role of Numerical Weather Prediction
M A Pedder, M Haile and A J Thorpe
September 1997

78. **Verification of the tracking technique used in an experimental cloud motion wind inferring system**
Z Wang, K A Browning and G A Kelly
October 1997

79. **A preliminary study of Fourier series analysis for cloud tracking with GOES high temporal resolution images**
Z Wang
October 1997

80. **Analysis of an ex-tropical cyclone after reintensifying as a warm-core extratropical cyclone**
K A Browning, G Vaughan and P Panagi
November 1997

81. **A JCMM overview of FASTEX IOPs**
S A Clough, H W Lean, N M Roberts, H Birkett, J-P Chaboureau, R Dixon, M Griffiths, T D Hewson and A Montani
January 1998

82. **Programs for PV inversion and modification**
Meral Demirtas
December 1997

83. **Release of potential shearing instability in warm frontal zones**
D Chapman and K A Browning
February 1998

84. **The European Cloud-Resolving Modelling Programme (EUCREM)**
Summary Report from the coordinator
P W White
April 1998

85. **A frontal wave database**
T D Hewson
April 1998

86. **Layering observed in dropsoundings from IOP 1 of Fronts 92**
S A Clough
May 1998

87. **Use of wind-shear displays for Doppler radar data**
D Chapman and K A Browning
May 1998

88. **Radar estimates of rainfall rates at the ground in bright band and non-bright band events**
T J Smyth and A J Illingworth
June 1998

89. **Correction for attenuation of radar reflectivity using polarisation data**
T J Smyth and A J Illingworth
June 1998

90. **The effects of convection on chemical reactions and precipitation scavenging**
Neil R Gimson
July 1998

91. **How to use the display program DISP**
Nigel Roberts
August 1998

92. **Conceptual models of cyclogenesis**
Adrian T Semple
August 1998

93. **Observations of oblate hail using dual polarisation radar and implications for hail detection schemes**
T J Smyth, T M Blackman and A J Illingworth
September 1998

94. **The semigeostrophic diagnosis of vertical motion. Part I: Formulation and co-ordinate transformations**
Mike A Pedder and Alan J Thorpe
September 1998

95. **The semigeostrophic diagnosis of vertical motion. Part II: Results for an idealised baroclinic wave life cycle**
Alan J Thorpe and Mike A Pedder
September 1998

Met Office Joint Centre for Mesoscale Meteorology Department of Meteorology
University of Reading PO Box 243 Reading RG6 6BB United Kingdom
Tel: +44 (0)118 931 8425 Fax: +44 (0)118 931 8791
www.metoffice.com